Spray Droplet Size and Velocity Measurement using Light-field Velocimetry

T. Nonn, V. Jaunet, S. Hellman
Dantec Dynamics A/S, Skovlunde, Denmark
thomas.nonn@dantecdynamics.com

Abstract

The past decade has seen considerable activity regarding light-field cameras and their application to photography. The ability to refocus images over a finite depth range has consequently led to interest in measuring the distance of objects from the camera. While originally developed for imaging structured opaque surfaces, interest has led to successful application in volumetric flow-fields using a commercially developed light-field camera. It is then expected that once particles are successfully imaged in 3D PIV flows, 2-phase and spray flows naturally follow. This paper focuses on the measurement of droplets in a spray using a light-field camera. While previous measurement techniques utilized a limiting 2D shadowing technique, measuring the size and velocity of droplets silhouetted from behind with uniform illumination, light-field measurements open the possibility of accessing the depth position, and thus the 3D position and velocity of individual droplets.

Introduction

The light-field technique has been described widely in literature [1,2,3], having its origins more than a century ago, but only in the last decade has momentum behind the technique increased, due to advances in optics, sensor resolution and manufacturing techniques. Currently the measurement of three-dimensional velocity components in experimental flow setups is carried out using multiple cameras, positioned around a fixed point and carefully aligned and calibrated. A single light-field camera opens up the possibility of a low-cost, robust and flexible alternative to multiple camera 3D measurement systems. A single camera capturing 3D events simplifies both physical access and calibration.

The general principle behind light-field camera can be described as follows: a micro-lens array placed closely to an image sensor, with the same f-stop as the main objective, reconstructs at selected positions virtual images representing focus planes within the measurement volume, as shown in figure 1. Particles appear in micro-images within several micro-lenses, at slightly different perspectives, allowing for depth determination. The downside of light-field cameras, however, is the loss of spatial resolution. The loss can be mitigated by applying multiple-focus micro-lens techniques used by a commercially available light-field camera. In such cases roughly 25 percent of the spatial resolution is retained, thus the 11 MP camera used in this study had an effective resolution of 2.6 MP. The depth resolution through the measurement volume is not constant, but increases monotonically with distance from the main objective, reaching a maximum in the far-field, as seen in figure 2. At the far-field the resolution is roughly 50% of the camera resolution.

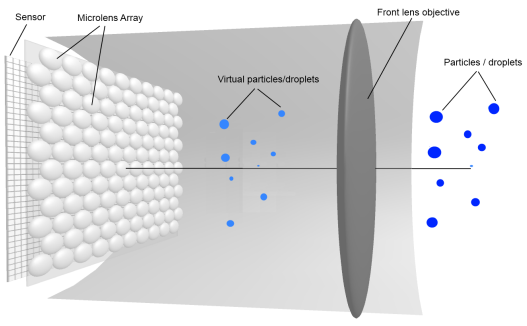

Figure 1 Optical schematic of light-field principle

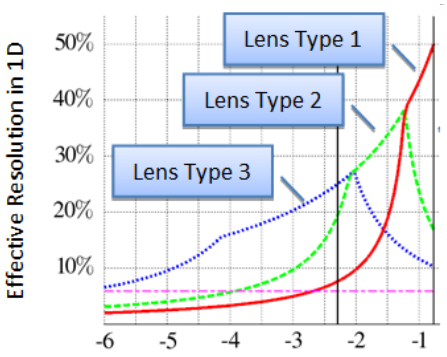

Figure 2 Resolution versus distance (Courtesy Raytrix)

Neighbouring micro-lenses act as local stereo systems, imaging large particles such as bubbles or droplets at slightly different perspectives, disclosing not only position in 3D space, but surface features as well. The depth of field of a light-field camera, or measurement depth, is limited by the f-stop of the micro-lens, which is also the f-stop of the main objective. Otherwise, the micro-images become heavily vig-netted or begin overlapping

neighbouring lenses. For the current camera and lens array configuration the f-stop was set to f8. To reduce the field of view a special magnification optics can be employed, so long as the f-stop can be maintained. Adding extension rings has the same effect, but moderately increases the f-stop as well. Typically a magnification of 5-7x is possible.

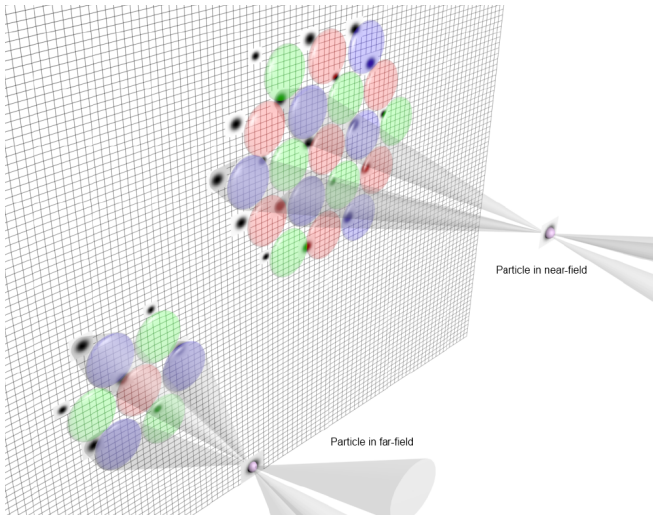

Figure 3 Near-field and far-field image projection of a particle onto image sensor.

Exploiting a micro-lens array (MLA) with multiple focal lengths, the depth of field can be extended, over a standard camera, up to a factor of seven. Figures 4-5 compares the imaging of particles in the micro lenses with those of target dots on a calibration plate. Note that in the microlens images below the degree of defocusing varies from lens to lens. Due to the hexagonal arrangement of the microlenses, as seen in figure 3, no two lenses of the same focal length are ever in contact. The images is some lenses are clearly more defocused than others. Images from lenses with the same focal lengths are examined together and compared against results from the other lens types. Lens type 3 resolves all images in the near-field, however, lens types 1 and 2 are needed to resolve the far-field.

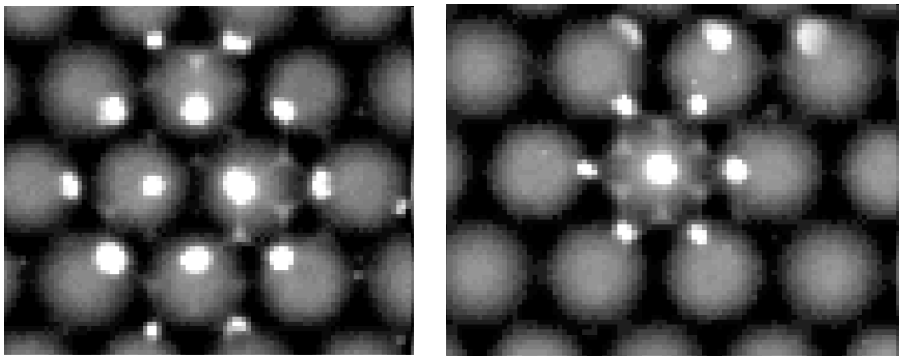

Figure 4 Near-field and far-field of a spherical particle (30 micron polymed)

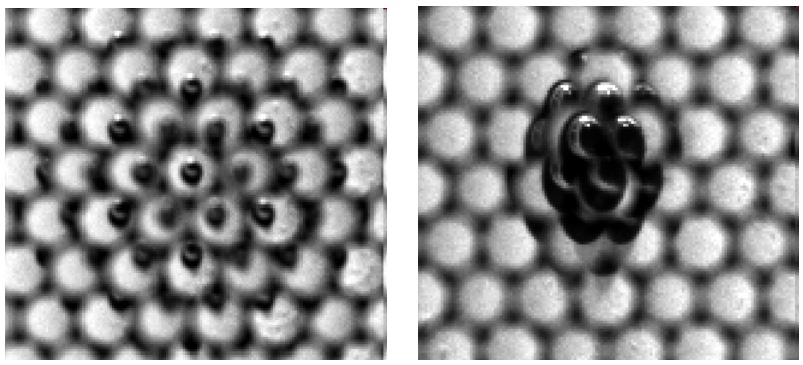

Figure 5 Near-field and far-field of a 2 mm target dot on a calibration plate

The typical strategy employed when determining particle depth positions is to first determine the position of image patches in each microlens and then by searching for similar or highly correlated patches in neighbouring lenses, and then applying epi-polar matching to estimate the position. A patch can be a particle or feature of a particle. By dividing a microlens image into four quadrants the possible positions a particle can have is reduced, assisting in depth determination.

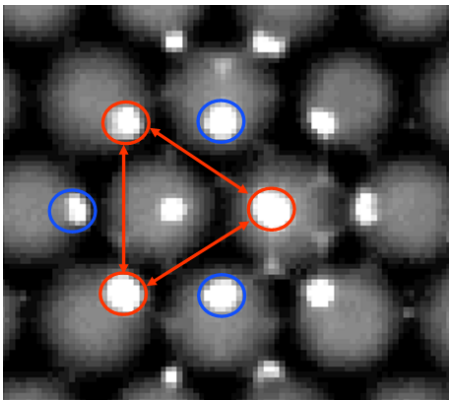

Figure 6 Image patches from lenses with similar focal lengths used for depth measurement.

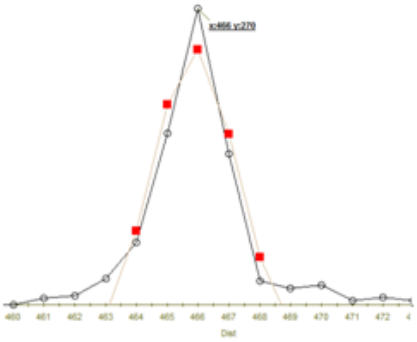

Figure 7 Gray-level intensity profile of an image patch.

The virtual depth is determined by comparing the position of patches taken from microlenses with the same focal lengths, as shown in figure 6. The microlens system giving the highest correlation is used to finally determine the depth. Subpixel improvement of the position is possible by applying a Gaussian fit over the intensity profile of the patch, as seen in figure 7.

As in PIV, the determination of the velocity field of particles in a volume requires the acquisition of at minimum two light-field images acquired in rapid succession. The depth map determined for each image is then analysed individually for particle positions and then processed together to determine the velocity field and particle flow history. Depending on the operating mode of the camera used the velocity field can the be determined from particle tracking techniques, least-square methods (LSM) or three-dimensional cross-correlation techniques. In practice the light-field camera operates best in flows with low to medium seeding densities. In higher densities particles become difficult to resolve and occlusion makes tracking difficult.

Experimental Methods

The depth information provided by the light-field camera is not calibrated, and represents a virtual space specific to the optical construction of the lens array, which changes with focus and objective selection. It was found that main objectives with long focal lengths (i.e. greater than 100 mm) gave reasonably linear responses and larger working depths when comparing virtual depth response with actual depth. The virtual depth is defined as the ratio of distances between the microlens array and sensor and the main objective. Shorter focal lengths gave shorter working depths and a more parabolic response. One of the hallmarks of plenoptic imaging is the ability to focus the entire image, an all-in-one focus. This feature greatly simplifies the calibration of the camera. A calibration target with a regular dot pattern with a known scaling is placed diagonally through the volume so as to cover the working volume. Unlike multiple camera calibrations where the coordinate system is aligned with the target, the coordinate system here is rotated to match with the camera. The depth information along the calibration target is then fitted to the virtual depth response of the camera. The uncertainly in the depth measurements encountered in many cases was below 0.6 % of the full depth range. A working depth range of 4 cm would have an uncertainty below 0.2 mm. This is still much larger than the lateral resolution of the sensor but reasonable for measurements.

The investigation consisted of measuring droplets from an agricultural nozzle. A Raytrix light-field camera used in combination with a Dantec imaging system was used for acquisition of data. Illumination was provided by a pulsed shadow strobe combined with a diffuser. For comparison purposes, 2D measurements on the nozzle were also carried with a phase-Doppler (PDA) system, as seen in figure 8.

The imaging system was calibrated with a textured dot target commonly used in stereo PIV. The calibration process consists of three independent processes: (1) software alignment of the micro-lens array (MLA); (2) calibration of the depth space based on the pinhole model; (3) Matching of the depth response of the light-field camera with the depth determined from the target calibration. The entire calibration process consists of acquiring two

images: a target image and a white image. The white image functions as a mask to mark regions lying within a microlens. The calibration target is placed diagonally across the measurement volume. The focus is adjusted so that dots farthest from the camera are nearly in focus. As one moves to the near-field dots begin to occupy ever larger rings of lenses. The depth volume depends on the focal length of the objective selected and the working distance. The depth volume increases with working distance with a corresponding decrease in depth resolution.

The alignment process ensures that the lenses are properly specified in the software during the reconstruction of the focus images. The near-field lenses were identifiable from the slightly thicker vignetting (i.e. more defocused). The next step in the calibration requires that the object-to-image coordinate relationship be determined.. Instead of focusing on a particular plane the depth map determined from the light-field data is used to put all objects in an image in focus. In this case all of the dots on the target are focused, making target identification easier. This image is then processed using a pinhole camera model to extract a transformation between image and object space. This essentially contains all our scaling information for 3D measurements. Typical reprojection errors were on the order of 0.5 - 0.8 pixels. It is expected that this uncertainty can be improved using a specially designed target with a finer dot distribution.

The last step of the calibration involves matching the virtual depth values returned by the camera with the actual depth values determined by the camera model. It was found for longer focal length objectives (> 100 mm) the relationship between virtual depth and actual depth was approximately linear, as is evident in figure 9. For shorter focal length lenses the relationship was parabolic. Once the calibration procedure is complete the target used can be reconstructed in 3D as verification. Typical residuals for the fit were between 0.4 - 0.7.

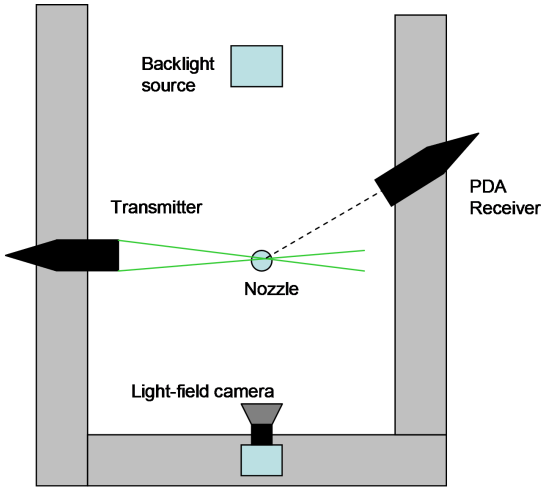

Figure 8 Layout of spray experiment.

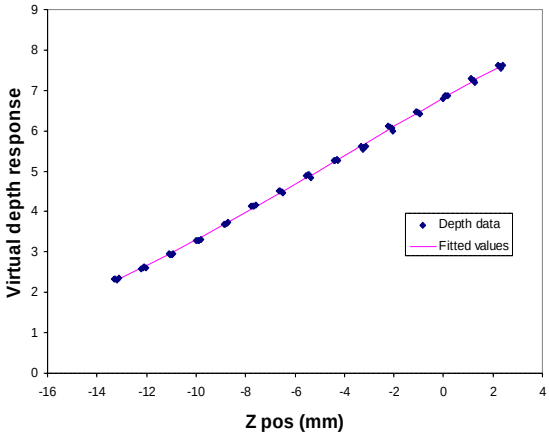

Figure 9 Calibration fit between virtual depth and measured depth.

Results and Discussion

For the current investigation a series of images was taken of the entire spray, as seen in figure 10. A color-mapped depth map of the whole spray gives a rough estimate of the distribution of droplets. Thereafter, several runs of 200 images were acquired from a subset of the whole field using the light-field camera, as shown in figures 11-15. In the subset ROI roughly 10-15 droplets were captured in each image. The working volume of the ROI subset was 3.8 cm x 2.5 cm x 1.4 cm. Within the ROI the focus plane could be moved to reveal droplet information, as seen in figures 11 and 12. A full focus image of the ROI can be seen in figure 13. The minimum diameter that could be effectively evaluated with the current optical setup was 10 microns. A higher resolution camera would have assisted in recovering more of the smaller droplets. A series of measurements with a PDA (phase-Doppler) system were carried out over a prescribed grid covering the spray profile. Three vertical slices of the volume giving 32 positions in total were used for comparisons. An example is given in Figure 16 comparing diameter distributions between the PDA and LF system. The minimum diameter that the LF system can measure is clearly evident. The lack of larger droplets was probably due to the limited number of images acquired.

A time-averaged result of the ROI data sequence, figure 15, shows the characteristic distribution of larger droplets in the outer region of the spray cone and the gradual falling off toward the center of the spray. The same can be seen in figure 17, a reconstruction of all droplets measured.

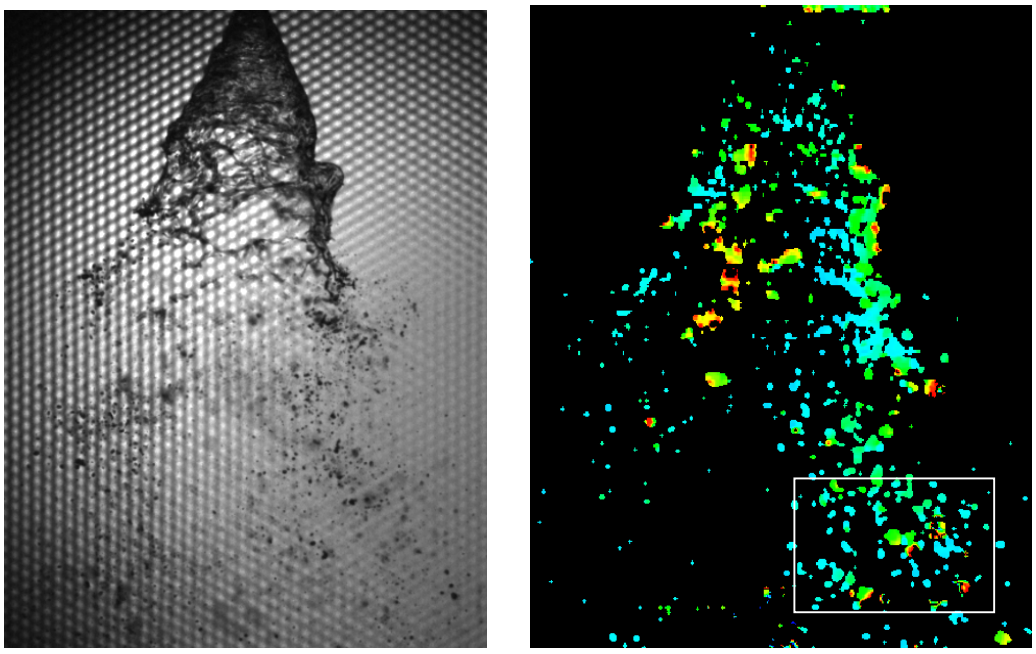

Figure 10 Focused image and corresponding color-mapped depth map of whole spray geometry from light-field data (Note ROI)

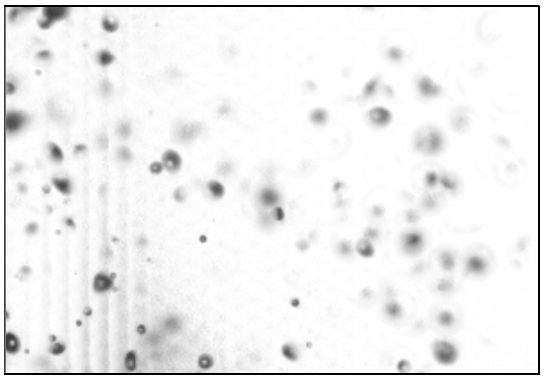

Figure 11 Focused droplet image at Z=-11 mm .

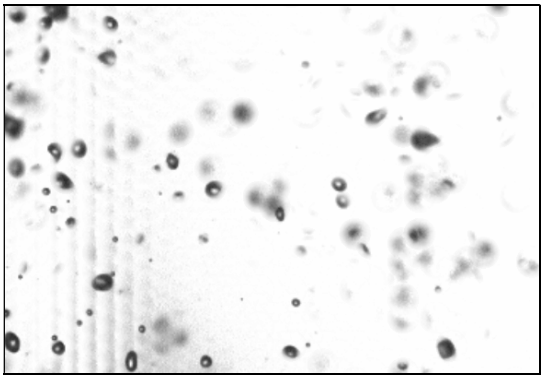

Figure 12 Focused droplet image at Z=0.2 mm

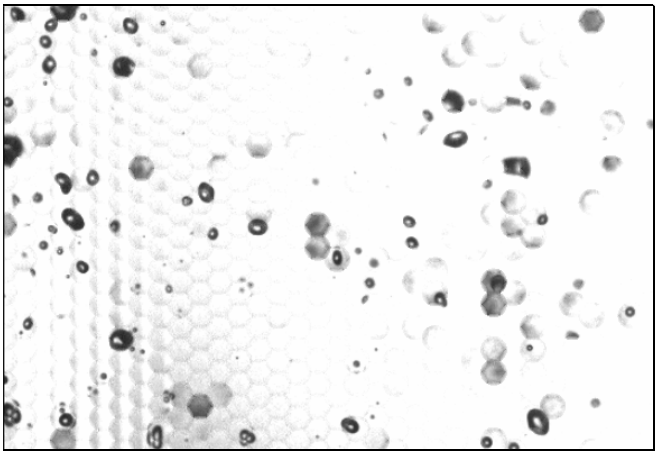

Figure 13 All-in-one focus image

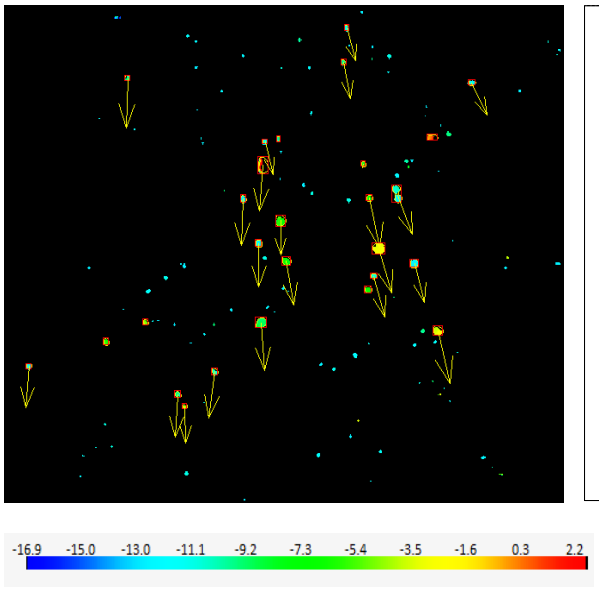

Figure 14 Sample frame (depth map) of droplets from one image within the ROI.

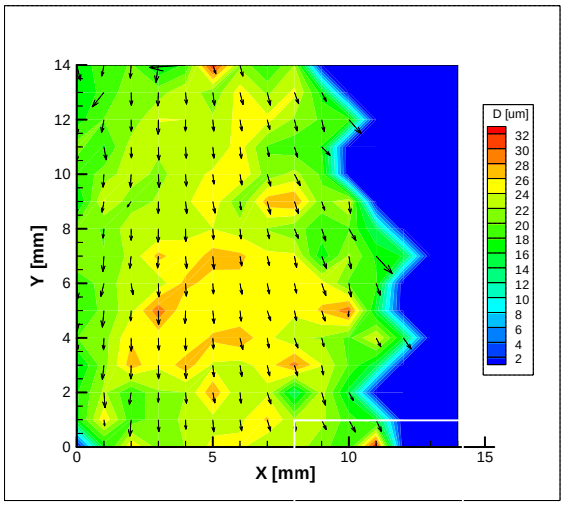

Figure 15 Time-averaged diameter mean and velocity (200 images) within ROI.

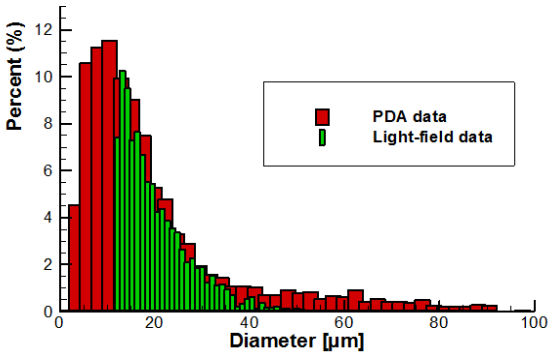

Figure 16 Comparison of droplet size histograms between PDA and Light-field imaging.

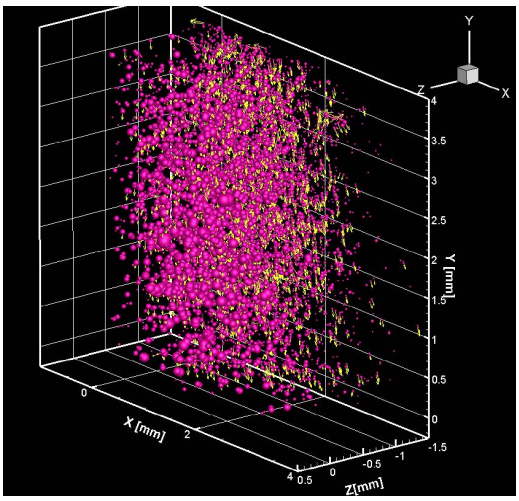

Figure 17 Volumetric reconstruction of all droplets (in ROI).

Summary and Conclusions

This investigation introduces the light-field camera to 3D spray measurement. It could be seen that not only droplets are useful subjects of this technology, but that the depth measurement could also extract positions of structures such as ligaments and the sheath of the spray. In the fully developed region of the spray comparisons with PDA were very encouraging. Current calibration techniques, while satisfactory, could do with some improvements. Future improvements in camera resolution will clearly improve the quality and accuracy of the results. The strength of the technique is clearly the ability to acquire 3D information from a single image. A persistent challenge in the measurements was magnification, which had a undesired affect of decreasing the aperture.

In general, the light-field camera simplifies the measurement and calibration process for 3D analysis. Another added value of LF over the shadow measurement technique is in resolving out-of-focus particles (figures 15-16), a persistent problem for conventional imaging. The investigation also focused on the uncertainties involved with LF measurement. This work is still considered preliminary. Other important parameters in droplet sizing, such as concentration, mass flux and others, are missing and will be part of a more thorough investigation in the future. However, these early results show promise and point to the practical usefulness of light-field technology in 3D measurement.

References

[1] T. Nonn, J. Kitzhofer and D. Hess, "Measurements in an IC-engine Flow using Light Field Volumetric Velocimetry", *Laser Appl. Fluid Flows*, Lisbon 2012.

[2] M. Levoy, "Light fields and computational imaging," Computer, vol. 39, pp. 46-55, 2006

[3] R. Ng, M. Levoy, M. Bredif, G. Duval, M. Horowitz, and P. Hanrahan, "Light field photography with a hand-held plenoptic camera," tech. rep., Stanford University, 2005

[4] Haeyoung Jeong, Kihyung Lee and Yuji Ikeda, "Investigation of the spray characteristics for a secondary fuel injector using a digital image processing method", Measurement Science and Tech.", vol. 18, pp.1591-1602, 2007.